Bioorganic Chemistry 53 (2014) 37–49

Contents lists available at ScienceDirect

Bioorganic Chemistry

journal homepage: www.elsevier.com/locate/bioorg

Substrate flexibility and reaction specificity of tropinone reductase-like short-chain dehydrogenases

Nicole Reinhardt [a], Juliane Fischer [b], Ralph Coppi [a], Elke Blum [a], Wolfgang Brandt [b], Birgit Dräger [a,*]

[a] Institute of Pharmacy, Faculty of Science I, Martin Luther University Halle-Wittenberg, Hoher Weg 8, D-06120 Halle, Germany
[b] Department of Bioorganic Chemistry, Leibniz Institute of Plant Biochemistry, Weinberg 3, D-06120 Halle, Germany

ARTICLE INFO

Article history:
Received 14 November 2013
Available online 7 February 2014

Keywords:
Tropinone reductase-like enzyme
Protein structure homology modeling
NAD(P)(H) specificity
SDR
Virtual screening

ABSTRACT

Annotations of protein or gene sequences from large scale sequencing projects are based on protein size, characteristic binding motifs, and conserved catalytic amino acids, but biochemical functions are often uncertain. In the large family of short-chain dehydrogenases/reductases (SDRs), functional predictions often fail. Putative tropinone reductases, named tropinone reductase-like (TRL), are SDRs annotated in many genomes of organisms that do not contain tropane alkaloids. SDRs *in vitro* often accept several substrates complicating functional assignments. *Cochlearia officinalis*, a Brassicaceae, contains tropane alkaloids, in contrast to the closely related *Arabidopsis thaliana*. TRLs from *Arabidopsis* and the tropinone reductase isolated from *Cochlearia* (CoTR) were investigated for their catalytic capacity. In contrast to CoTR, none of the *Arabidopsis* TRLs reduced tropinone *in vitro*. NAD(H) and NADP(H) preferences were relaxed in two TRLs, and protein homology models revealed flexibility of amino acid residues in the active site allowing binding of both cofactors. TRLs reduced various carbonyl compounds, among them terpene ketones. The reduction was stereospecific for most of TRLs investigated, and the corresponding terpene alcohol oxidation was stereoselective. Carbonyl compounds that were identified to serve as substrates were applied for modeling pharmacophores of each TRL. A database of commercially available compounds was screened using the pharmacophores. Compounds identified as potential substrates were confirmed by turnover *in vitro*. Thus pharmacophores may contribute to better predictability of biochemical functions of SDR enzymes.

1. Introduction

Tropinone reductases are short-chain dehydrogenases/reductases (SDRs) specific for tropane alkaloid biosynthesis. In many genomes of organisms that do not contain tropane alkaloids, tropinone reductase-like genes are annotated due to sequence similarities. The SDR superfamily comprises over 47,000 sequences in gene and protein databases [1], among them over 300 SDR crystal structures in the PDB [2]. The SDR nomenclature initiative [3] divides the members of the SDR superfamily into seven types, wherein classical SDRs with a length of about 250 amino acids form the largest group in eukaryota and bacteria. SDR enzymes typically show a low pairwise sequence identity between 20% and 30%, but they share the three-dimensional structure [4,5]. A single-domain Rossmann-fold consisting of a central β-sheet with seven segments, flanked by three to four α-helices on each side is a folding pattern typical for nucleotide binding enzymes. Classical SDR enzymes are mostly NAD(P)(H) dependent carbonyl-alcohol oxidoreductases (EC 1.1.1.-) [4]. Binding of the cofactors NAD(H) or the phosphorylated NADP(H) is determined by few amino acids in the N-terminal glycine-rich motif (TGXXXGXG) and by few amino acids at the C-terminal end of the second β-sheet [6]. Classical SDRs share a catalytic triad comprising serine, tyrosine and lysine. The triad was extended into a tetrad for many SDRs by a conserved asparagine, which takes part in a proton relay system through a backbone bound water molecule [5,7]. Serine stabilizes the substrate by a hydrogen bond, and tyrosine acts as catalytic acid, from which a proton is transferred to the substrate carbonyl. Lysine forms a hydrogen bond with the

Abbreviations: CoTR, tropinone reductase of *Cochlearia officinalis*; Cotr, tropinone reductase of *Cochlearia officinalis* (cDNA); DsTRI, tropine forming tropinone reductase of *Datura stramonium*; DsTRII, pseudotropine forming tropinone reductase of *Datura stramonium*; HMBC, heteronuclear multiple-bond correlation; HSQC, heteronuclear single-quantum correlation; Rt, retention time; SDR, short-chain dehydrogenase/reductase; TMS, tetramethyl silane; TR, tropinone reductase; TRL, tropinone reductase-like short-chain dehydrogenase/reductase.

* Corresponding author. Fax: +49 345 55 27021.
E-mail address: birgit.draeger@pharmazie.uni-halle.de (B. Dräger).

http://dx.doi.org/10.1016/j.bioorg.2014.01.004
0045-2068/

nicotinamide-ribosyl moiety (2′OH) of the cofactor and thereby lowers the pK_a of the tyrosine hydroxyl, promoting the proton transfer [7,8]. The substrate binding sites at the C-terminus of SDRs accept a wide array of substrates from simple aliphatic alcohols and sugars to complex alkaloid precursors, steroids and xenobiotics [9]. Individual SDRs often accept several substrates, which renders functional predictions complicated.

Tropinone reductase-like SDRs (TRLs) belong to the classical SDRs and were combined in group SDR65C by the SDR nomenclature initiative [3]. SDR65C currently contains over 350 members (http://www.sdr-enzymes.org, table of the SDR65C family, accessed July 2013). Genes of plants and microorganisms are annotated as (putative) tropinone reductases based on a sequence similarity of >50% to proven tropinone reductases from Solanaceae and sequence motif comparisons using Hidden Markov models. Typically, tropinone reductases (TRs) catalyze the stereospecific reduction of the alkaloid metabolite tropinone in the tropane alkaloid biosynthesis of Solanaceae, such as *Atropa belladonna* or *Datura stramonium* (Fig. 1). The product of TRI (EC 1.1.1.206) is tropine (α-tropanol) necessary for tropane alkaloid formation. TRII (EC 1.1.1.236) forms the β-alcohol pseudotropine, a precursor for nortropane alkaloids like calystegines [10]. In the Brassicaceae *Cochlearia officinalis*, the tropane alkaloid cochlearine and several calystegines were identified [11,12]. A SDR encoded by *cotr* (EMBL ID: **AM748271**) reduced tropinone with catalytic specificities different from Solanaceae TRs. The tropinone reductase isolated from *C. officinalis* (CoTR) forms both alcohols, tropine and pseudotropine, and catalyzes their oxidation back to tropinone (Fig. 1). The CoTR is so far the only functional TR identified from Brassicaceae. In the UniProt database [13] 16 genes of *Arabidopsis thaliana* (Brassicaceae) were annotated as "putative tropinone reductase", "tropine dehydrogenase" or "tropinone reductase I". These genes were later named "tropinone reductase-like SDR", because *A. thaliana* does not contain any tropane or nortropane alkaloids, and tropinone reducing activity appeared implausible in the plant [11]. Most of those genes are arranged in tandem on chromosome 2, spanning over positions At2g29150 to At2g29370.

The uncertainty of denomination and of functional assignment of *A. thaliana* SDRs prompted us to investigate the catalytic capacities of TRLs. For functional examination, two TRLs with an amino acid identity of 79% to the proven tropinone reductase from *C. officinalis* were chosen. They are encoded at loci *at2g29350* (EMBL ID: **AY081642**) and *at2g29150* (EMBL ID: **DQ056552**). In addition, one TRL encoded at *at2g29330* (EMBL ID: **BT005864**) was investigated, which is more distant with 61% overall identity to CoTR. The enzymes are subsequently named by their loci in the *Arabidopsis* genome. They were examined for their catalytic activities towards several small carbonyl and hydroxyl groups containing compounds. Sequence similarity to known TRs enabled construction of homology models of the enzymes At2g29150, At2g29330, At2g29350 and CoTR and substrate docking. Experimentally proven substrate structures then afforded the frame for pharmacophore descriptions that allowed screening a large database of commercially available compounds for identification of further substrates for the TRLs.

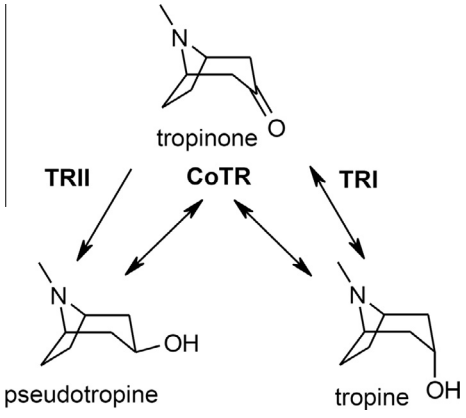

Fig. 1. Tropinone reduction: branch point in tropane and nortropane alkaloid biosynthesis. TRI, tropine forming tropinone reductase; TRII, pseudotropine forming tropinone reductase; CoTR, tropinone reductase from *Cochlearia officinalis*.

2. Results and discussion

2.1. Substrate binding site and tropinone reduction

First, tropinone-reducing capacity of the TRLs was examined by docking tropinone into the active site of protein models of the enzymes. Equally, tropinone was applied as substrate *in vitro*. In contrast to successful docking into homology models of the enzymes and a position of the carbonyl group adapted for reduction, none of *A. thaliana* TRLs reduced tropinone or oxidized tropine or pseudotropine *in vitro*. So far reduction of tropinone appears to be limited to tropinone reductases from Solanaceae and to CoTR from *C. officinalis*. In addition, a TRL protein called DnTR1 from *Dendrobium nobile* (Orchidaceae) reduced tropinone to tropine [14]. Crystallization and site-directed mutagenesis of TRI and TRII of *Datura stramonium* identified E156 in DsTRII and V168 at the equivalent position in DsTRI as the important amino acids for the stereospecific reduction of tropinone to either tropine or pseudotropine [15,16]. Compared to DsTRI and DsTRII the active sites of CoTR and the *Arabidopsis* TRL enzymes are more constricted. All Brassicaceae enzymes show a gap in the C-terminal region which forms the active site (position 221 in CoTR, Fig. 2), yet CoTR is a tropinone-reducing enzyme. The homology model of CoTR showed tropinone docked different from *Datura* TRs and in contact with Y209 [17]. In At2g29350, At2g29330 and At2g29150 hydrophobic phenylalanine or isoleucine residues are located at this position (Fig. 2, white on grey). As further space restriction, At2g29350 and At2g29150 contain a bulky tryptophane at the active site, where functional tropinone reductases contain a small glycine (black on yellow; Fig. 2). We conclude that bicyclic tropinone does not serve as substrate to TRL due to spatial hindrance of binding in spite of successful docking.

Tropinone reductases including CoTR are able to reduce ketones with structural similarity to tropinone (Fig. 3) like nortropinone, quinuclidin-3-one, and *N*-methyl- and *N*-propylpiperidin-4-one [17,19,20]. Except for At2g29330, the TRLs of this study did not reduce any of those compounds. The reducing activity of At2g29330 for tropinone-analogous substrates was too low for kinetic characterization.

In summary, these TRLs are no functional tropinone reductases. They neither reduce tropinone nor nitrogen-containing tropinone analogues, probably due to limited space in the binding pocket, although *in silico* docking of tropinone was possible.

2.2. Specificity of cofactor binding

The contrast between prediction of tropinone as substrate and the *in vitro* activity provoked to test how efficient substrates and cofactors for the TRLs overall may be predicted *in silico*. Kallberg et al. [6,21] developed an algorithm for prediction of cofactor specificity of classical SDRs, distinguishing NAD(H) and the phosphorylated forms. Basic amino acids like lysine (K31 in DsTRI) or arginine (R19 in DsTRII) in the glycine-rich motif (Table 1, Fig. 2) stabilize the 2′-phosphate-group of NADP(H) by ionic interactions. Arginine (R53 in DsTRI) at the first loop position after the second β-sheet

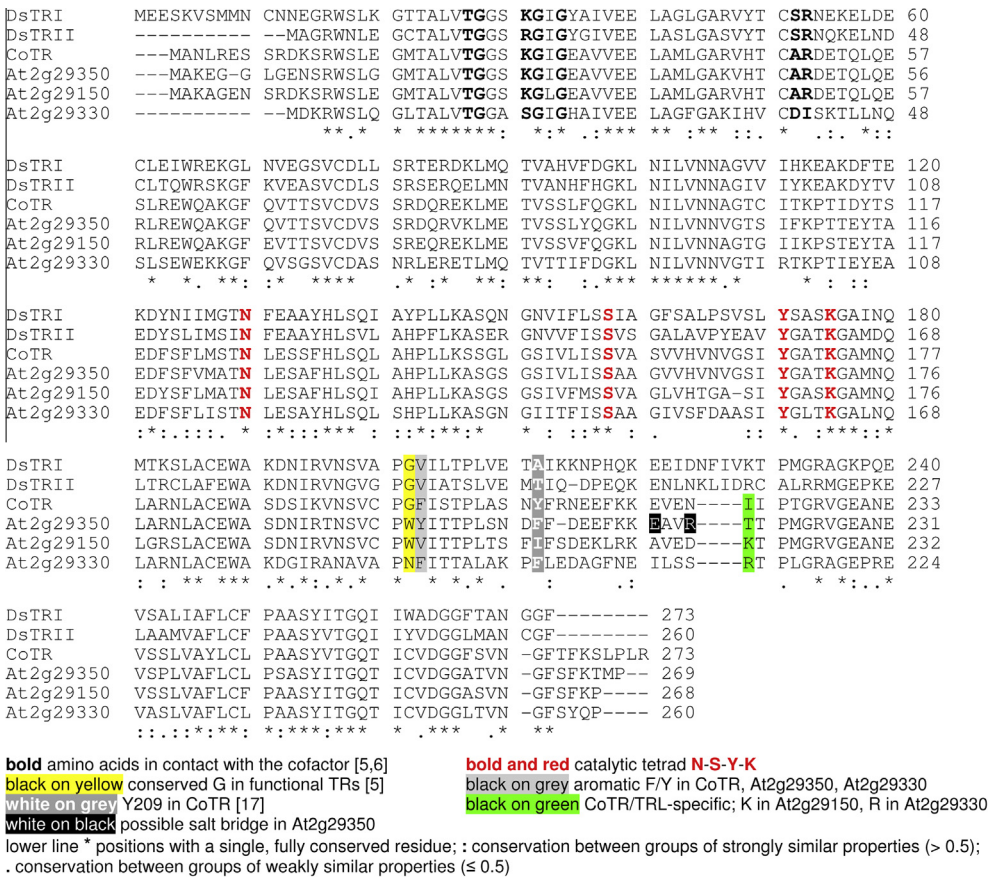

Fig. 2. Multiple sequence alignment of DsTRI, DsTRII, CoTR, At2g29350, At2g29150 and At2g29330 performed with protein weight matrix Gonnet in ClustalW2 [18].

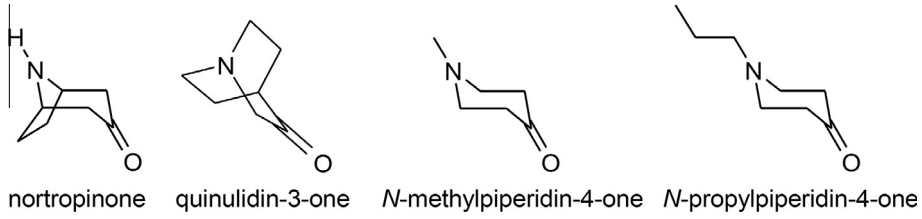

Fig. 3. Tropinone-like ketones are substrates for TRs and CoTR, but not or scarcely accepted by *A. thaliana* TRLs of this study.

Table 1
Amino acid positions determining NAD(P)(H) preference according to [6,21] are black and bold in Fig. 2.

Enzymes	Predicted	Amino acid positions		
DsTRI	NADP(H)	K31	S52	R53
DsTRII	NADP(H)	R19	S40	R41
CoTR	NADP(H)	K28	A49	R50
At2g29350	NADP(H)	K27	A48	R49
At2g29150	NADP(H)	K28	A49	R50
At2g29330	NAD(H)	S19	D40	I41

equally interacts with that 2′-phosphate. Enzymes containing two basic amino acid residues at those positions were assigned to the NADP(H) preferring subfamily cP3 within the classical SDRs [6]. These criteria classify the tropinone reductases DsTRI (EMBL ID: **L20473**), DsTRII (EMBL ID **L20474**) and CoTR, At2g29350 and At2g29150 as NADP(H)-specific (Table 1).

Cofactor turnover was tested with 3-methylcyclohexanone and its corresponding alcohol. These substrates were accepted by all enzymes and enabled comparative testing. Cofactor turnover kinetics were measured at the pH optima for the reduction of 3-methylcyclohexanone (pH 5.0) and for the oxidation of 3-methylcyclohexanol (pH 8.0 for At2g29350; pH 9.5 for the other three enzymes). The *in vitro* preference for NADP(H) concurred with the cofactor prediction for DsTRI, DsTRII [22] and for At2g29350 and At2g29150. The enzymes did not catalyze reduction or oxidation with NAD(H) (Table 2). The detection limit for the photometric assay was an absorption difference of 0.001 units per minute, corresponding to a specific activity of 30 pkat mg^{-1} (k_{cat} $9 \cdot 10^{-4}$ s^{-1}) with 100 µg protein per assay. Values below this detection limit were termed "no activity". CoTR catalyzed reactions with both cofactors. The predicted cofactor NADPH had a better affinity (K_m), but turnover was faster with NADH resulting in a higher overall catalytic efficiency (k_{cat}/K_m). NAD(H) may be bound despite of the two basic amino acids (K28; R50) in CoTR without ionic interactions at the ribose ring adjacent to adenine and thus with decreased affinity. For most SDR enzymes an ordered bi–bi mechanism with the cofactor binding first and leaving last is postulated [23–26]. The turnover number k_{cat} for the reaction

Table 2
Kinetic properties for cofactor acceptance of CoTR and TRL enzymes. Reduction measured with 3-methylcyclohexanone and NAD(P)H at pH 5.0; oxidation measured with 3-methylcyclohexanol and NAD(P) at pH 9.5 (pH 8.0 for At2g29350). Data are the mean of at least 4 replicates ± standard deviation.

Cofactor	Kinetic parameters	CoTR	At2g29350	At2g29150	At2g29330
NADPH	K_m (μM)	78.3 ± 7.9	30.1 ± 2.6	7.1 ± 1.4	297.2 ± 45.0
	k_{cat} (s^{-1})	1.01 ± 0.03	1.06 ± 0.02	$0.35 \pm 4 \cdot 10^{-3}$	0.70 ± 0.01
	k_{cat}/K_m (s^{-1} mM^{-1})	12.9	35.22	49.3	2.36
NADH	K_m (μM)	666.5 ± 2.0			59.3 ± 7.4
	k_{cat} (s^{-1})	11.80 ± 0.22	No activity	No activity	0.34 ± 0.04
	k_{cat}/K_m (s^{-1} mM^{-1})	17.7			5.73
NADP	K_m (μM)	27.9 ± 1.8	37.8 ± 2.3	4.8 ± 0.4	
	k_{cat} (s^{-1})	$0.16 \pm 2 \cdot 10^{-3}$	$0.28 \pm 3 \cdot 10^{-3}$	$0.02 \pm 2 \cdot 10^{-4}$	No activity
	k_{cat}/K_m (s^{-1} mM^{-1})	5.73	7.41	4.19	
NAD	K_m (μM)	963.5 ± 41.7			15.0 ± 1.1
	k_{cat} (s^{-1})	$0.45 \pm 9 \cdot 10^{-3}$	No activity	No activity	$0.03 \pm 3 \cdot 10^{-4}$
	k_{cat}/K_m (s^{-1} mM^{-1})	0.47			2

comprises all phases in the examined reaction direction and is limited by the slowest reaction step. If binding or release of the cofactors is the rate-limiting step, a higher k_{cat} for CoTR catalyzing the reactions with less tightly bound NAD(H) is explicable. Indeed, velocity limitation by cofactor release was excellently shown for two aldose reductases (aldo–keto reductase family, EC 1.1.1.21) by fluorescence stopped-flow techniques [27,28] and for dihydrofolate reductase, a member of the SDRs [29]. The enzyme At2g29330 is predicted to prefer NAD(H). Enzymes without basic residues in the cofactor binding region belong to the NAD(H) preferring subfamily cD1d if, in addition, a negatively charged aspartate is located at the C-terminal end of the second β-sheet. Instead of basic residues for NADP(H) binding At2g29330 contains isoleucine (I41) and a serine (S19) (Table 1, Fig. 2) that forms hydrogen bonds to the 2′- and 3′-hydroxyl groups of the adenine ribose moiety of NAD(H). The aspartate (D40 in At2g29330, Fig. 2) is thought to repulse a negatively charged 2′-phosphate group on that ribose in NADP(H) [21,30]. *In vitro*, At2g29330 accepted both cofactors. A protein model of At2g29330 allowed binding of both, NADH and NADPH as cofactors, because a clash of the negatively charged aspartate with the 2′-phosphate of NADPH was avoided by a rotation of D40 away from NADPH (Fig. 4). The NADPH phosphate group appeared exposed to solvent and did prevent binding to the At2g29330. Similar to CoTR, NADPH was less tightly bound than NADH in At2g29330, and the turnover was doubled compared to NADH (Table 2). Substrate oxidation reaction was measureable with NAD only. Turnover for substrate reduction was elevenfold faster than oxidation with NAD when both

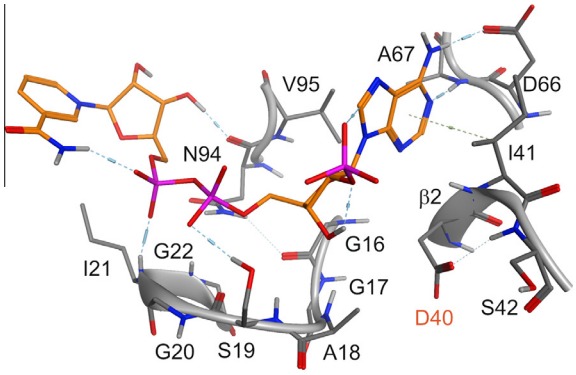

Fig. 4. Cofactor binding site in At2g29330 with NADPH. The GGXXGXG-motif and the three amino acids, S19, D40 (highlighted in orange) and I41 at the second β-sheet (β2) mentioned in Table 1 are shown. Orange, carbon of NADPH; grey, carbon of amino acids; blue, nitrogen; red, oxygen; purple, phosphor; grey, hydrogen, nonpolar hydrogen not shown.

reactions were measured at optimal pH, indicating that substrate reduction was the preferred direction of the enzyme catalysis at substrate and cofactor saturation.

In summary, flexible cofactor acceptance by CoTR and At2g29330 and faster turnover with the non-predicted cofactor *in vitro* were in contrast to predictions *in silico*, but the respective enzymes exhibited higher affinity (lower K_m) for the predicted cofactor.

2.3. Reduction of small flexible lipophilic carbonyls

Considering that substrate binding sites in the enzyme models appear small and are lined by hydrophobic amino acids and that substrates with a charged nitrogen atom were mostly not accepted, lipophilic carbonyl compounds were tested as substrates. Small aliphatic structures like acetone and acetaldehyde were reduced by CoTR and At2g29350 but not by At2g29150 (data not shown). As the substances are volatile their reduction could not be reliably quantified under the assay conditions. Aliphatic carbonyl structures with five carbon atoms like pentanal (valeraldehyde) and 2,4-dimethylpentan-3-one were tested as substrates. Aliphatic monoterpenes like citronellal and citral (mixture of neral and geranial) and the monocyclic terpene analogues 3- and 4-methylcyclohexanone (Fig. 5) were included. Docking of these compounds to the four enzyme models predicted them as substrates. CoTR and the TRLs catalyzed the reduction and oxidation of all small lipophilic substrates with distinct pH optima for the respective reaction direction (Table 3).

The reductions of pentanal and citronellal by CoTR and of pentanal by At2g29330 were analyzed with the equation for uncompetitive substrate inhibition (Fig. 6). Here, simultaneous reverse reactions were excluded, because CoTR did not oxidize pentanol alone at pH 5.0 and pH 9.5 (data not shown). It is assumed that the aldehyde substrates or the alcohol products act as inhibitors of the reductase reaction by forming non-productive complexes with the enzymes, as was postulated for a dihydroflavonol 4-reductase from grape vine [31]. Substrate inhibition of CoTR by pentanal and citronellal was measured in the same order of magnitude. In contrast, the reduction of citronellal was catalyzed by all TRLs with moderate turnover and affinities (K_m 75–264 μM) and no substrate inhibition effects appeared.

The reduction of aldehydes and ketones at acidic pH values was always faster (k_{cat}) than the oxidation of the corresponding alcohols at basic pH values (Table 3). Reverse reactions in the assays were minimized by pH differences of 3–4.5 pH units (reduction: pH 5.0; oxidation: pH 9.5 or pH 8.0 for At2g29350). Still, oxidation of 4-methylcyclohexanol at pH 9.5 by CoTR was paralleled by reduction of the product 4-methylcyclohexanone, as observed

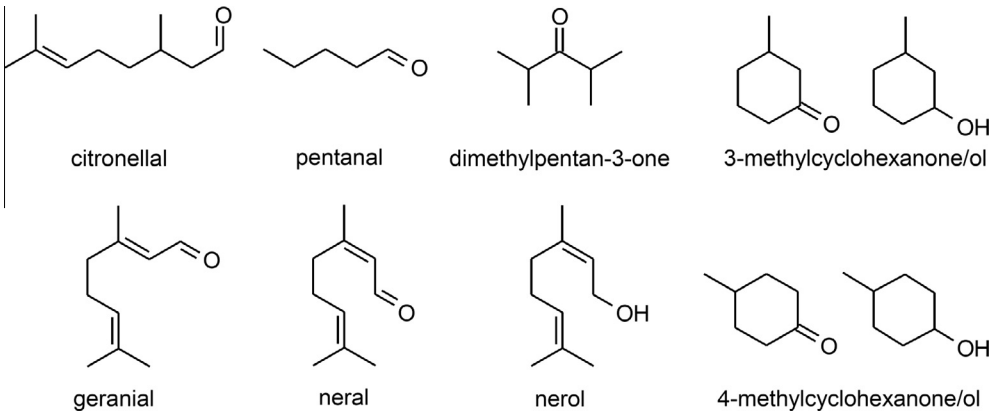

Fig. 5. Small flexible lipophilic structures used as substrates for reduction or oxidation.

Table 3
Kinetic properties of CoTR and TRL enzymes for small flexible lipophilic carbonyls. Data are the mean of at least 4 replicates ± standard deviation.

Substrate	Kinetic parameters	CoTR	At2g29350	At2g29150	At2g29330
Citronellal	K_m (μM)	app. 71.4[SI]	264.1 ± 18.1	74.5 ± 8.7	108.7 ± 11.5
	k_{cat} (s^{-1})	app. 0.16[SI]	0.47 ± 0.01	0.56 ± 0.02	0.13 ± 4 · 10^{-3}
	k_{cat}/K_m (s^{-1} mM^{-1})	2.24	1.78	7.52	1.2
Pentanal	K_m (μM)	app. 74.1[SI]	612.0 ± 58.8		64.6[SI] ± 2.1
	k_{cat} (s^{-1})	app. 0.16[SI]	0.02 ± 1 · 10^{-3}	+	0.09[SI] ± 0.02
	k_{cat}/K_m (s^{-1} mM^{-1})	2.16	0.03		1.39
Dimethylpentan-3-one	K_m (μM)	76.9 ± 9.1			389.7 ± 67.8
	k_{cat} (s^{-1})	0.57 ± 0.02	+	+	0.02 ± 6 · 10^{-4}
	k_{cat}/K_m (s^{-1} mM^{-1})	7.41			0.05
Nerol	K_m (μM)	26.0 ± 1.3	98.1 ± 4.7	67.4 ± 3.8	464.1 ± 29.2
	k_{cat} (s^{-1})	0.06 ± 6 · 10^{-4}	0.08 ± 1 · 10^{-3}	0.01 ± 2 · 10^{-4}	0.02 ± 6 · 10^{-4}
	k_{cat}/K_m (s^{-1} mM^{-1})	2.31	0.82	0.15	0.04
3-Methylcyclohexanone	K_m (μM)	24.1[RR] ± 3.2	504.9 ± 33.7	559.5 ± 46.5	56.7 ± 6.3
	k_{cat} (s^{-1})	2.34[RR] ± 0.09	1.61 ± 0.03	0.34 ± 7 · 10^{-3}	0.20 ± 4 · 10^{-3}
	k_{cat}/K_m (s^{-1} mM^{-1})	97.1	3.19	0.61	3.53
3-Methylcyclohexanol	K_m (μM)	57.2 ± 2.6	373.4 ± 18.8	315.2 ± 14.2	61.9 ± 7.6
	k_{cat} (s^{-1})	0.17 ± 2 · 10^{-3}	0.17 ± 2 · 10^{-3}	0.02 ± 3 · 10^{-4}	0.03 ± 6 · 10^{-4}
	k_{cat}/K_m (s^{-1} mM^{-1})	2.97	0.46	0.06	0.48
4-Methylcyclohexanone	K_m (μM)	5.1[RR] ± 0.9	463.0 ± 41.8	106.0 ± 11.0	71.5 ± 7.4
	k_{cat} (s^{-1})	3.54[RR] ± 0.10	0.78 ± 0.02	0.09 ± 2 · 10^{-3}	0.20 ± 3 · 10^{-3}
	k_{cat}/K_m (s^{-1} mM^{-1})	694.12	1.68	0.85	2.8
4-Methylcyclohexanol	K_m (μM)	29.2[RR] ± 2.3	328.8 ± 21.4	378.5 ± 39.6	63.3 ± 7.8
	k_{cat} (s^{-1})	0.17[RR] ± 4 · 10^{-3}	0.03 ± 6 · 10^{-4}	0.01 ± 3 · 10^{-4}	0.03 ± 6 · 10^{-4}
	k_{cat}/K_m (s^{-1} mM^{-1})	5.82	0.09	0.03	0.47

[RR] Reverse reaction measurable under assay conditions.
[SI] Substrate or product inhibition; + product confirmed by GC–MS, but no kinetic characterization possible; *app.* apparent values (Fig. 6).

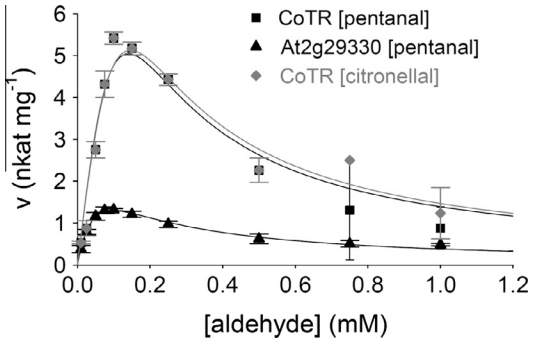

Fig. 6. Substrate inhibition of CoTR by pentanal (black square) and citronellal (grey diamond) and of At2g29330 by pentanal (black triangle).

before for tropine oxidation [17]. Similarly, reverse reaction was measured with reduction of methylcyclohexanones by CoTR at pH 5.0. The kinetic data fitted best to the equation for "uncompetitive substrate inhibition" and were marked (RR, Table 3). In summary, CoTR and TRLs reduced a variety of small lipophilic carbonyl compounds as predicted from docking, yet with highly different kinetic characteristics.

2.4. Stereospecificity in reducing cyclic monoterpenes

The reduction of cyclohexanones encouraged to use natural terpene ketones as substrates. Mono- and sesquiterpenes for *in vitro* tests were selected by their commercial availability (Fig. 7). Except for verbenone [32,33] the selected terpenes do not occur naturally in Brassicaceae, yet some of them proved to be good substrates. (−)-Menthone was reduced by all enzymes (Table 4, and Fig. S1A). Affinities were low for (−)-menthone compared to other menthone reducing SDRs (Table S1), but turnover rates were in the same range as those of a menthone reductase from peppermint (MpMMR [34]) and of a broad-substrate oxidoreductase AaRed1 from annual wormwood [35]. At2g29330 catalyzed (−)-menthone

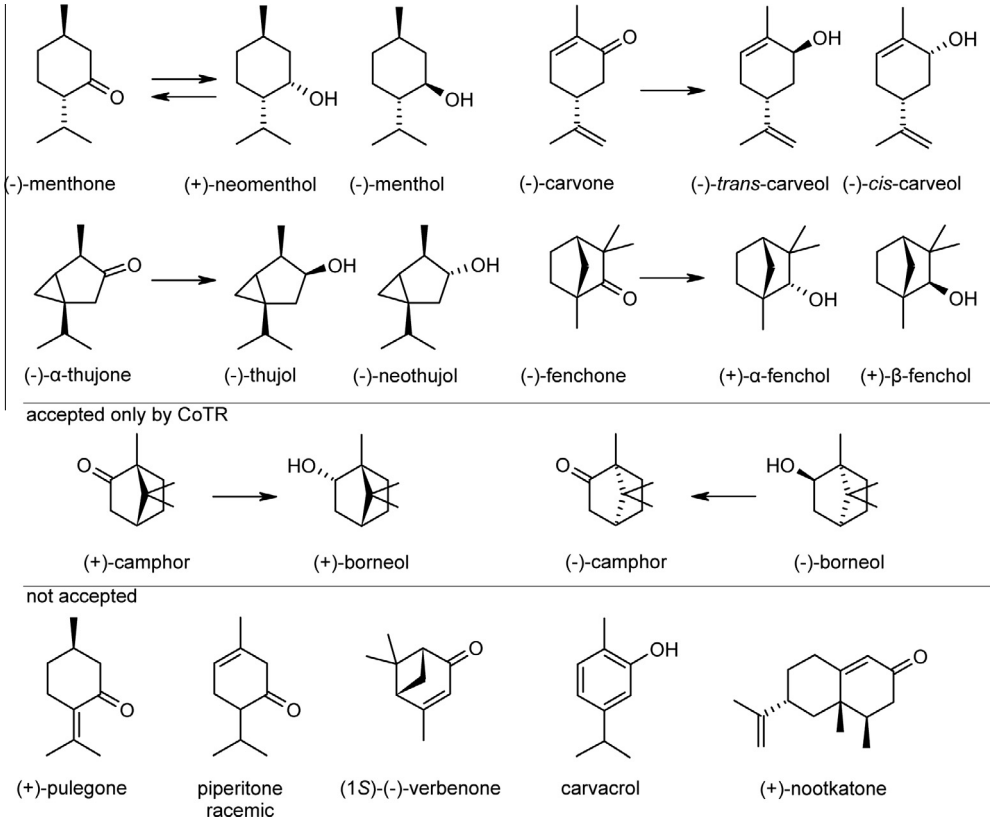

Fig. 7. Terpene structures tested as substrates with resulting products.

Table 4
Kinetic properties of CoTR and TRL enzymes for cyclic monoterpenes. Reduction at pH 5.0; oxidation at pH 9.5 (At2g29350 pH 8.0). Data are the mean of at least 4 replicates ± standard deviation. + product confirmed by GC–MS, but no kinetic characterization possible.

Substrate	Kinetic parameters	CoTR	At2g29350	At2g29150	At2g29330
(−)-Menthone	K_m (μM)	282.2 ± 30.8	118.1 ± 8.1	452.4 ± 41.3	
	k_{cat} (s^{-1})	0.31 ± 9 · 10^{-3}	0.83 ± 0.01	0.19 ± 5 · 10^{-3}	+
	k_{cat}/K_m (s^{-1} mM^{-1})	1.1	7.03	0.42	
(+)-Neomenthol	K_m (μM)	20.3 ± 2.9		113.0 ± 7.4	
	k_{cat} (s^{-1})	0.02 ± 3 · 10^{-4}	+	0.02 ± 3 · 10^{-4}	+
	k_{cat}/K_m (s^{-1} mM^{-1})	0.99		0.18	
(−)-Menthol	K_m (μM)		50.1 ± 2.6		
	k_{cat} (s^{-1})	+	0.04 ± 6 · 10^{-4}	No activity	No activity
	k_{cat}/K_m (s^{-1} mM^{-1})		0.8		
(−)-Carvone	K_m (μM)	62.3 ± 7.7	75.7 ± 7.6	1830.0 ± 170.0	
	k_{cat} (s^{-1})	0.12 ± 3 · 10^{-3}	0.17 ± 4 · 10^{-3}	0.47 ± 0.02	No activity
	k_{cat}/K_m (s^{-1} mM^{-1})	1.93	2.25	0.26	
(−)-α-Thujone	K_m (μM)	65.0 ± 6.3	1340.0 ± 210.0	891.5 ± 86.0	
	k_{cat} (s^{-1})	0.46 ± 9 · 10^{-3}	0.11 ± 7 · 10^{-3}	0.25 ± 9 · 10^{-3}	No activity
	k_{cat}/K_m (s^{-1} mM^{-1})	7.08	0.08	0.28	
(−)-Fenchone	K_m (μM)	36.2 ± 5.1			
	k_{cat} (s^{-1})	0.07 ± 2 · 10^{-3}	+	+	No activity
	k_{cat}/K_m (s^{-1} mM^{-1})	1.93			
(+)-Camphor	K_m (μM)	1038.1 ± 267.8			
	k_{cat} (s^{-1})	0.06 ± 7 · 10^{-3}	No activity	No activity	No activity
	k_{cat}/K_m (s^{-1} mM^{-1})	0.06			
(−)-Camphor	K_m (μM)				
	k_{cat} (s^{-1})	No activity	Not determined	Not determined	Not determined
	k_{cat}/K_m (s^{-1} mM^{-1})				
(−)-Borneol	K_m (μM)	126.2 ± 7.7			
	k_{cat} (s^{-1})	0.09 ± 1 · 10^{-3}	No activity	No activity	No activity
	k_{cat}/K_m (s^{-1} mM^{-1})	0.71			

reduction slowly and reduced none of the other cyclic terpenes. A basic arginine at position 213 (Fig. 2 black on green, Fig. 8a1) in the substrate binding site may hinder lipophilic monoterpene substrates from binding. The high K_m value for monoterpenes in At2g29150 may be caused by a lysine residue at position 221 equivalent to R213 in At2g29330 (Fig. 2 black on green, Fig. 8b1). Lysine is more flexible than arginine and may rotate away from the active site more easily, allowing binding of monoterpenes although with decreased affinity.

For confirmation of R213 influence on substrate binding, 1,3- and 1,4-cyclohexanedione as ligands with a second acceptor group were docked (Fig. 8a1). Energy minimizations for both structures showed positions adapted to serve as substrates. Enzymatic reduction with At2g29330 *in vitro* confirmed 1,4-cyclohexanedione as substrate with affinity and turnover ($K_m = 105.6 \pm 4.1$ μM; $k_{cat} = 0.28 \pm 2 \cdot 10^{-3}$ s^{-1}) similar to citronellal and monocyclic ketones. As expected, the other three enzymes showed low affinity and turnover for 1,4-cyclohexanedione; none of them catalyzed the reduction of 1,3-cyclohexanedione in quantifiable amounts. Except for At2g29330, (−)-carvone, (−)-α-thujone and (−)-fenchone were reduced by the enzymes (Table 4). CoTR was most active with monoterpene substrates and reduced (−)-fenchone and (+)-camphor, whereas (−)-borneol was oxidized by CoTR. Terpenes with double bonds in the ring or directly associated to the ring like (+)-pulegone, piperitone, (1*S*)-(−)-verbenone, (+)-nootkatone or the aromatic carvacrol were no substrates for any of the enzymes. When the diasteromeric reduction products of (−)-menthone were applied as oxidation substrates, (+)-neomentol was preferred by CoTR and At2g29150, while At2g29350 preferred (−)-menthol (Table 4).

The diastereomeric reduction products were assigned *via* GC–MS comparing them to reference standards and literature data (Table 5). Also, reduction products of (−)-α-thujone were elucidated by ^{13}C and ^{1}H NMR in comparison to published data [36,37]. The product ratio (%) in Table 5 is independent from the catalytic efficiency (Table 4). At2g29150 reduced the monoterpenes stereospecifically, in contrast to At2g29350 that formed both diasteriomeric alcohols of (−)-menthone, (−)-carvone, (−)-α-thujone and (−)-fenchone (Table 5). CoTR is stereospecific for (−)-carvone and (−)-α-thujone reduction and non-stereospecific for the reduction of (−)-menthone and (−)-fenchone. The oxidation of the alcohols (−)-menthol and (+)-neomenthol largely concurred with the preferred alcohol product; the enzymes selectively oxidized those alcohols that were produced during (−)-menthone reduction (Table 4, Fig. S1B).

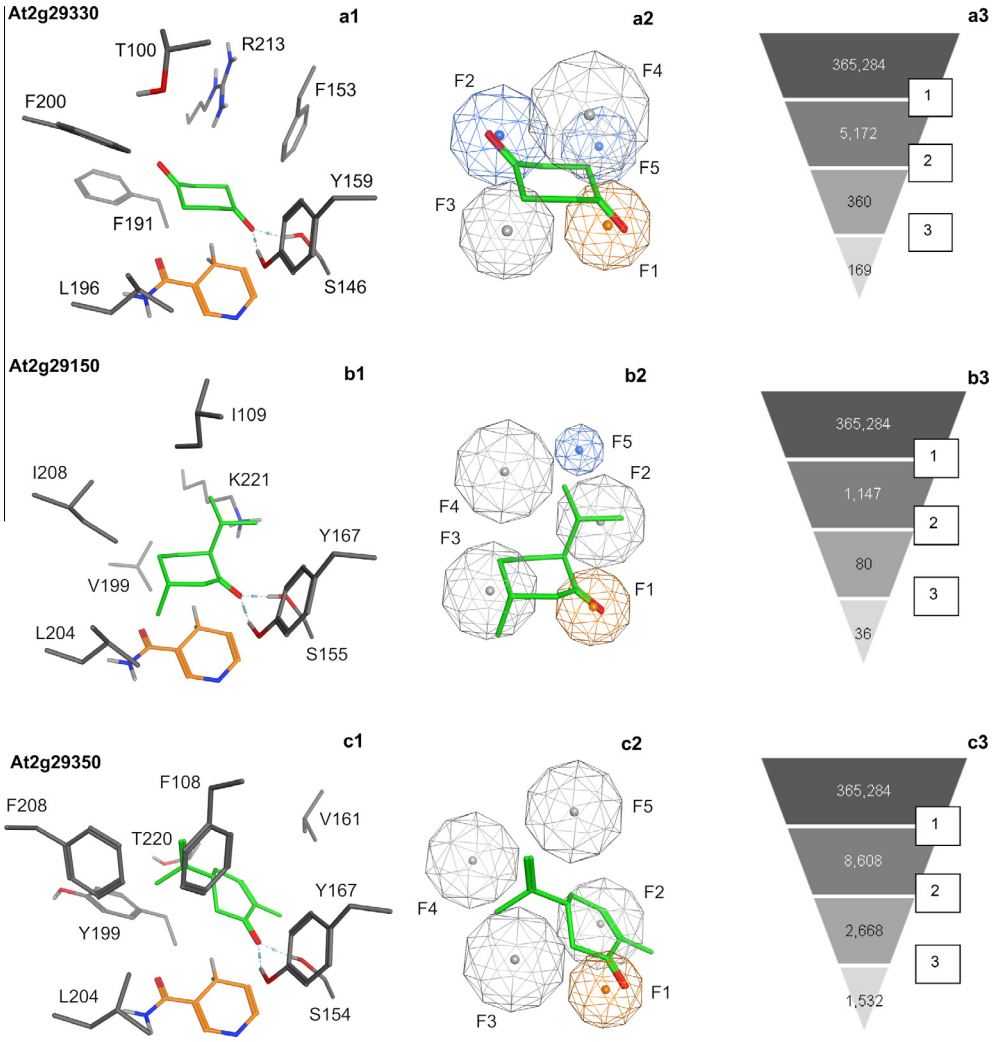

Fig. 8. Active site with ligands (first column, ligand: green carbon atoms, nicotinamide: orange carbon atoms), pharmacophore (second column), and screening route (third column): At2g29330 with 1,4-cyclohexanedione (first row), At2g29150 with (−)-menthone (second row) and At2g29350 with (−)-carvone (third row). Pharmacophores – orange: acceptor and no donor and no anion, blue: acceptor (and for At2g29330 alternatively a hydrophobic feature), grey: hydrophobic feature. Screening route: 1. step: pharmacophore search and manual check, 2. step: docking and second search with absolute position, 3. step: manual check.

Table 5
In vitro product formation analyzed by GC–MS (% product ratio), – no activity.

Monoterpene substrate and reduction products		CoTR	At2g29350	At2g29150	At2g29330
(−)-Menthone	(+)-Neomenthol	40	10	100	100
	(−)-Menthol	60	90	0	0
(−)-Carvone	(−)-*trans*-Carveol	100	80	100	–
	(−)-*cis*-Carveol	0	20	0	–
(−)-α-Thujone	(−)-Thujol	100	80	100	–
	(−)-Neothujol	0	20	0	–
(−)-Fenchone	(+)-α-Fenchol	40	35	95	–
	(+)-β-Fenchol	60	65	5	–

In summary, natural terpene ketones are substrates for CoTR, At2g29350 and At2g29150. At2g29350 acts as an unspecific reductase providing both diastereomeric alcohols from the prochiral ketones, and At2g29150 is an enantiospecific enzyme. Monoterpenes containing carbon bridges are accepted predominantly by CoTR with a substrate binding site large enough to accommodate also tropinone.

2.5. Virtual screening

The enzyme 3d-models of the active sites together with experimentally confirmed substrates enabled pharmacophore constructions (Fig. 8, first column). Pharmacophores of the enzymes were intended to identify substrates by screening small compound libraries. The array of ligands selected by pharmacophores should facilitate functional assignments *in silico* and enable targeted biochemical testing. The pharmacophores of At2g29150 and At2g29350 were constructed using monoterpenes with good turnover as ligands. Pharmacophore features of At2g29330 were based on 1,4-cyclohexanedione as ligand, because it provided better *in vitro* turnover (Section 2.4) than the monoterpenes. Additional features (e.g. F5 in At2g29330) were chosen according to the type of amino acids in the substrate binding site. The resulting pharmacophores (Fig. 8, second column) are composed of five features (F1–F5, Table 10).

Feature 1 (F1, orange) provides the position for the carbonyl function of the ligands located in an acceptable distance to the C4-hydrid of NAD(P)H and to the catalytic tyrosine and serine enabling reduction. F1 has the same position and function in all pharmacophores. It is defined as proton acceptor without donor and anionic characteristics to exclude hydroxyl and carboxyl groups in this position. All models contain several hydrophobic features (grey). Experimental results for monoterpenes and 1,4-cyclohexanedione confirmed the hypothesis of a less hydrophobic active site in At2g29330 represented in the pharmacophore by only two hydrophobic features (F3, F4). Additional proton acceptor or hydrophobic features F2, F5 (blue spheres) defined the area of the flexible R213 (Fig. 2, black on green). Hydrophobic features of At2g29150 and At2g29350 differed only slightly in position and size. In At2g29150, F5 is defined as acceptor (blue) representing K221. The corresponding position of At2g29350 is T220 building a hydrogen bond to the backbone of A217 (not shown) and thereby appearing more hydrophobic. In the outer active site of At2g29350, a glutamate (E216, Fig. 2, white on black) is represented as hydrophobic feature (F5, grey), because a salt bridge to a nearby arginine is formed (R219, Fig. 2, white on black), which reduces the proton acceptor ability (not shown). The pharmacophores served for screening the MOE collection of structures of commercially available compounds (Fig. 8, third column). *In vitro* experiments revealed reduction as the preferred reaction direction, therefore only structures with carbonyl functions and a molecular weight <400 Da were selected, which reduced structures from >650,000 to 365,284. In the first step, pharmacophore searches with all defined features were carried out. Afterwards esters and amides without additional keto or aldehyde function were deleted as they cannot be substrates for SDR; although it is known they act as inhibitors for some reductases [38,39].

In the second step the remaining structures were docked, and the absolute position of the resulting conformations was checked with the pharmacophores, where four out of five features with essential F1 were set as compulsory. In the third step all resulting docking arrangements were manually checked for a keto or aldehyde function in the reactive position F1. The screening procedure with the three pharmacophores finally resulted in highly different numbers of hits for each TRL. Also, the structures of the hits were partially different for each pharmacophore, in spite of the features for the pharmacophores being quite similar (Table 10). For example, compounds with a 1,4-benzoquinone structural element as exclusive carbonyl for reduction were selected by the pharmacophore of At2g29330 to a larger extent than by At2g29350. Five 1,4-benzoquinone derivatives were selected among 169 hits for At2g29330, while only one 1,4-benzoquinone was selected for At2g29350 among 1532 hits. Instead, the pharmacophore of At2g29350 found 18 1,4-naphtoquinones as substrates to be reduced, indicating a more spacious binding site. Some scaffolds were recognized in all three pharmacophores, e.g. flavonoids. Flavanone, 2′-hydroxyflavanone, 6-hydroxyflavanone, and *trans*-chalcone were selected for *in vitro* tests (Fig. 9). All three enzymes catalyzed the reduction of those four substrates *in vitro*, but reduction activity appeared different. The enzyme At2g29350 reduced all four flavonoids more effectively than At2g29330. Activity of At2g29150 ranged between the two others (Table S2). Thus, the pharmacophore screening identified new classes of substrates for the *Arabidopsis* TRLs. Further new substrate scaffolds were suggested by pharmacophore screening (Fig. 8, third column) and wait for *in vitro* testing. It should be emphasized that the first array of substrates screened here was limited to commercially available compounds and represents only a small amount of all possible ligands.

3. Conclusions

Numerous SDR genes resulting from genome sequencing projects are annotated by similarities to known enzymes, but predictions of substrate acceptance and biochemical function remain difficult up to now [9]. This is exemplified by SDR-encoding genes of *Arabidopsis* named "tropinone reductases" or "tropinone reductase-like". None of the investigated enzymes reduced tropinone or oxidized corresponding alcohols when tested *in vitro*. However, all *Arabidopsis* TRLs reduce small lipophilic ketones and several monoterpene ketones and oxidized the corresponding alcohols. Stereospecificity and stereoselectivity towards monoterpenes appear useful for biotechnological applications. Monoterpenes are widely used as additives for food, cosmetics, or pharmaceutical products.

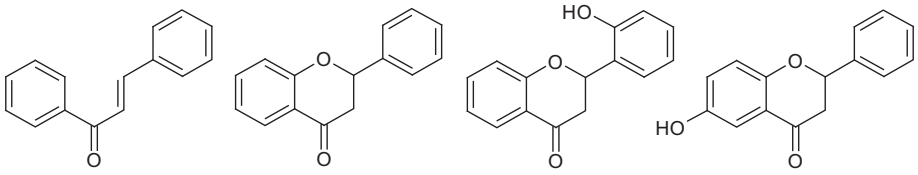

Fig. 9. Scaffolds predicted by pharmacophore screening and experimentally proven substrates for TRLs.

Pure enantiomers of (−)-thujol and (−)-neothujol cannot be purchased, and (−)-*trans*-carveol is available only as mixture of *cis* and *trans* diastereomers in unknown ratio. Given their high protein yield by heterologous expression in microorganisms, TRLs provide new options for enantiospecific synthesis of oxidized terpenes and further natural compounds. After cloning into microorganisms, TRL capacities can be utilized either in the whole cells or as isolated enzymes. One limitation for oxidoreductases in biocatalysis is the costs of cofactors, NADH demanding ca. 10% of the price of the phosphorylated NADPH. In SDRs, cofactor preference can be predicted by amino acids located in the conserved cofactor binding site [6,21]. Experimental tests of the predicted cofactors basically confirmed the predictions but *in vitro*, two of four SDRs accepted both cofactors with different affinities. Knowledge of amino acids important for cofactor preference enables site-directed mutagenesis to shift cofactor preference from NADP(H) to NAD(H), efficiently [30,40–42].

The substrate acceptance of enzymes like TRLs is often not indicated correctly in sequence data bases, and their potential as multi-substrate and enantiospecific biocatalysts is not yet largely exploited. The team play of *in silico* and *in vitro* studies can help to improve annotation of function. *In silico* screening with pharmacophores derived from protein models combined with ligand docking can help to predict potential ligands that can serve for biochemical testing. The structure database search with pharmacophores may lead to new, unexpected ligands, as demonstrated above for the *Arabidopsis* TRLs. This approach opens the way for better predictability of the biochemical capacities of SDRs.

4. Experimental procedures

4.1. Chemicals

(+)-α-Fenchol, (+)-camphor, (−)-borneol, isoborneol, (−)-carvone, (−)-α-thujone, (1*S*)-(−)-verbenone, 2,4-dimethylpentan-3-one, quinuclidin-3-one hydrochloride, *N*-methyl- and *N*-propylpiperidin-4-one, pentanal, (−)-menthone, (+)-neomenthol, (+)-pulegone, (+)-nootkatone, *trans*-chalcone, 2′-hydroxyflavanone and 6-hydroxyflavanone were purchased from Sigma–Aldrich (Taufkirchen, Germany). (−)-Menthol, (−)-fenchone, piperitone, carvacrol, citronellal, citral, nerol, tropine, tropinone, NAD, NADH disodium salt and NADP disodium salt were ordered from Carl Roth (Karlsruhe, Gemany). NADPH tetrasodium salt was purchased from Applichem (Darmstadt, Germany). Methylcyclohexanones and methylcyclohexanols were obtained from Merck Schuchardt (Hohenbrunn, Germany). Flavanone was purchased from Acros Organics (Geel, Belgium). Nortropinone hydrochloride was a gift from F. Bischoff (Boehringer-Ingelheim, Germany). Pseudotropine was synthesized by B. Dräger according to Nickon and Fieser [43]. All chemicals were obtained with high purity. The cofactors, tropinone and analogues and the methylcyclohexanones and methylcyclohexanols were used as tenfold concentrated stock solutions in purified water; all other chemicals were dissolved in methanol, because of their hydrophobicity and were used as 20-fold concentrated stock solutions.

4.2. Cloning, synthesis and purification of recombinant proteins

CoTR was cloned in vector pET21d (Novagen), providing a C-terminal hexahistidine-tag, and the construct was transformed into *E. coli* Rosetta-gami (DE3) (Novagen) as described previously [17]. The coding sequences of *at2g29350* and *at2g29330* were amplified by RT-PCR (SuperScript II Reverse Transcriptase Kit, Invitrogen; Pfu DNA Polymerase, Fermentas) from isolated RNA from a whole-plant of *A. thaliana* ecotype Columbia [44] and for *at2g29150* by PCR using vector PENTR221-At2g29150 purchased from ABRC DNA Stock Centre (Columbus, USA) as template. Primers used for PCR of *at2g29350* were forward 5′-GCATGCGCAAAGGAAGGG GGCTTG-3′ (SphI) and reverse 5′-CTGCAGTTATGGCATAGTCTTG AAGGAAAAACC-3′ (PstI), of *at2g29150* forward 5′-GGATCCGCT-AAAGCAGGAGAAAACTCGAGAG-3′ (BamHI) and reverse 5′-CTG-CAGCTAAGGCTTGAAAGAGAA-GCCATTC-3′ (PstI) and of *at2g29330* forward 5′-GGATCCGATAAAAGGTGGAGTCTCCAAG-3′ (BamHI) and reverse 5′-GTCGACCTATGGCTGATATGAGAAGCC-3′ (SalI). Amplified fragments were cloned into vector pQE30 (Qiagen), providing a N-terminal hexahistidine-tag. The recombinant plasmids were transformed into *E. coli* M15[pREP4] (Qiagen) and protein synthesis was induced at an OD600 of 0.7–0.9 with 1 mM IPTG (Fermentas) for 5 h at 37 °C. Rosetta-gami (DE3) cells containing CoTR were incubated for 16 h at 25 °C after induction with 1 mM IPTG. Cells were harvested by centrifugation at 5,000 rpm and 4 °C for 10 min and resuspended in lysis buffer (300 mM NaCl, 50 mM $NaH_2PO_4 \times 2H_2O$, 10 mM imidazole, pH 8.0) containing protease inhibitor cocktail for use in purification of histidine tagged proteins (Sigma–Aldrich). Cells were lysed on ice for 30 min with lysozyme (32 mg L^{-1}; Applichem) and subsequent sonification for 1 min (Branson sonifier duty 50%). After addition of DNase I (51 U mL^{-1} buffer; Applichem) and incubation for 10 min at room temperature, the cell suspension was centrifuged at 13,000 rpm at 4 °C for 45 min. Protein was purified from the supernatant on 1 mL Ni-HisTrap HP columns (GE Healthcare) with ÄKTA explorer 100 protein chromatography system (Pharmacia). The system was equilibrated with binding buffer (300 mM NaCl, 50 mM $NaH_2PO_4 \times 2H_2O$, 10 mM imidazole, pH 8.0). After application of the lysate, the column was washed with 20 column volumes of binding buffer. An imidazole gradient from 10 to 500 mM over 20 column volumes in elution buffer (300 mM NaCl, 50 mM $NaH_2PO_4 \times 2H_2O$, 500 mM imidazole, pH 8.0) eluted fractions containing the purified hexahistidine fusion proteins. Buffer was exchanged on PD-10 columns (GE Healthcare). CoTR, At2g29350 and At2g29330 were stored in buffer A (20 mM potassium phosphate buffer, 100 mM NaCl, 1 mM DTT and 20% glycerole, pH 7.0) and At2g29150 in buffer B (same as A but pH 7.5). Purity of all proteins was checked with SDS–PAGE on 15% polyacrylamide gels [45], all enzymes appeared as single bands with a size of ca. 30 kDa. Protein concentrations were determined using Bradford assay [46]. Typically, 1.7–2.2 μg μL^{-1} fusion protein was achieved, corresponding to total amounts of 16–28 mg L^{-1} culture medium. The enzyme solution was divided into 250–350 μL portions, frozen with liquid nitrogene (Air Liquide) and stored at −80 °C until usage.

4.3. Enzyme characterization and activity assays

Oxidoreductase activity was measured spectrophotometrically following NAD(P)H consumption (reduction) or accumulation (oxidation) at 340 nm and 30 °C [17]. An initial substrate screening assay of 1 mL contained 10–100 μg mL^{-1} enzyme, 200 μM NADP(H) or NAD(H) for At2g29330 and 1–5 mM of the substrate, either as tenfold concentrated stock solution in water or as 20-fold concentrated stock solution in methanol, in 100 mM buffer (Photometer: Shimadzu UV-160A, reduction: potassium phosphate buffer pH 6.4 for basic ligands, citrate phosphate buffer pH 5.0 for lipohilic substrates; oxidation: for At2g29350 tris–HCl buffer pH 8.0, glycine–NaOH buffer pH 9.5 for the other enzymes). A blank assay contained the same mixture without substrate. The detection limit was set to ±0.001 absorption units per minute, corresponding to a specific activity of 30 pkat mg^{-1} (k_{cat}: $9 \cdot 10^{-4}$ s^{-1}) for 100 μg enzyme. For kinetic characterization, the assay was limited to 200 μL. 96-well plates and a microplate reader with automatic injection system (Infinite F200PRO, Tecan) were used. The change of absorption per minute was measured after starting the reaction by injection of the cofactor (with variable substrate concentrations) or of the substrate (with variable cofactor conditions). Calibration was done with 0.001–0.8 mM NADPH. The resulting linear regression equation was also used for analysis of NAD(H) dependent oxidoreductions; both dinucleotides share the same extinction coefficient (6.22 mM^{-1} cm^{-1}). The pH-dependency was measured for the reduction of 5 mM 3-methylcyclohexanone and for the oxidation of 5 mM 3-methylcyclohexanol in assays containing 5–10 μg mL^{-1} enzyme and 200 μM cofactor in 100 mM of different buffers with increasing pH-values in 0.5 steps. Buffers for reduction were citrate phosphate buffer pH 4.5–5.5, potassium phosphate buffer pH 5.5–7.5 and tris–HCl buffer pH 7.5–9.0. For oxidation potassium phosphate buffer pH 6.4–7.5, tris–HCl buffer pH 7.5–9.0 and glycine–NaOH buffer pH 9.0–10.0 were used. For each condition four separate samples and two blank assays were provided.

Kinetics for cofactor acceptance were measured with 5 mM 3-methylcyclohexanone at pH 5.0 (reduction) and 5 mM 3-methylcyclohexanol at pH 9.5 (pH 8.0 for At2g29350) for the oxidation. Cofactor concentrations varied from 0.01 to 0.40 mM for NAD(P)H and from 0.01 to 1.00 mM for NAD(P). Depending on enzyme activity and type of substrate, kinetic assays contained 1–20 μg mL^{-1} enzyme, 200 μM cofactor and typically 0.01–5.0 mM substrate in 100 mM buffer pH 5.0 for reduction or pH 9.5 or 8.0 (At2g29350) for oxidation and 5% (v/v) methanol, if 20-fold concentrated methanolic stock solution was used. For each substrate concentration four independent samples and four blank assays were measured. Substrate affinities (K_m), inhibition constants (K_i) and velocities (V_{max}) were calculated using SigmaPlot 10 (Systat Software Inc.).

4.4. Product analysis by GC–MS

The reaction products for oxidoreduction were identified by GC–MS. One assay with 0.5 mL contained 50–100 μg mL^{-1} enzyme, 1 mM cofactor and 1 mM substrate in 5% (v/v) methanol and 100 mM of the appropriate buffer. Assays with the same composition, containing boiled protein (95 °C for 10 min) were used as blanks. All assays were covered with a layer of 0.25 mL n-hexane (aldehydes and monoterpenes) or ethyl acetate (pentanal, 2,4-dimethylpentan-3-one) and were incubated at 30 °C for 1 h. After vigorously shaking, the organic phase was separated by centrifugation (1 min at 13,000 rpm) and used for analysis with GC–MS (GC-2010 and GCMS-QP2010S; Shimadzu) on a DB-5 silica column (FS-Supreme-5 ms, 30 m × 0.25 mm, 0.25 μm, CS). Separation conditions: initial temperature 60–150 °C at 4 °C min^{-1}, 1 min at 150 °C, 150–245 °C at 15 °C min^{-1}, 3 min at 245 °C; carrier gas: Helium 1 mL min^{-1}, injection: 1 μL splittless, transfer line temperature: 250 °C; ion source temperature: 200 °C, absolute detector voltage: 1.5 kV, scanning: 50–400 atomic mass units. For the sesquiterpene (+)-nootkatone the temperature program was adapted: initial temperature 60–150 °C at 15 °C min^{-1}, 1 min at 150 °C, 150–245 °C at 10 °C min^{-1}, 3 min at 245 °C. For the more volatile substances pentanal and 2,4-dimethylpentan-3-one the temperature program was adapted: 50–90 °C at 2 °C min^{-1}; scanning 30–100 atomic mass units. Products were identified by the NIST 2008 spectrum library and authentic standards, as far as available, comparing retention times and major fragments with % abundance (Table 6).

4.5. Reduction of flavanones and trans-chalcone

One assay with 0.5 mL contained 50 μg mL^{-1} enzyme, 1 mM NADPH (NADH for At2g29330) and 1 mM substrate (6-hydroxyflavanone 0.75 mM) in 5% (v/v) methanol and 100 mM citrate phosphate buffer pH 5.0. Assays with the same composition, containing boiled protein (95 °C for 10 min) were used as blanks. The assays were incubated at 30 °C for 1 h whilst gently shaking (700 rpm) and were finally extracted with 200 μL ethyl acetate. The organic phase was directly injected to the HPLC system (Agilent series 1100) and analyzed on a C18 column (Merck LiChrospher 100 RP18 LiChroCart 125-4, 5 μm, 4 × 125 mm) in a solvent system consisting of A phosphoric acid/water 0.5/99.5 v/v and B acetonitrile with a gradient of 15% B to 100% B in 20 min. Column temperature was 25 °C; flow was 1 mL min^{-1}; injection volume was 10 μL.

Table 6
Retention times (Rt) and major fragments of oxidoreduction products analyzed with GC–MS.

Reaction products	Rt (min)	Major fragments (% abundance)					Standard or reference
Citronellol	13.14	69 (100)	95 (37)	109 (13)	123 (16)	156 (3)	NIST 2008
Pentanol	3.40	31 (65)	41 (68)	42 (100)	55 (61)	70 (27)	NIST 2008
Dimethylpentan-3-ol	4.58	41 (2)	43 (31)	55 (62)	72 (13)	73 (100)	NIST 2008
Nerol	13.13	69 (100)	93 (21)	111 (5)	123 (9)	139 (2)	Nerol
Geraniol	14.00	69 (100)	93 (11)	111 (5)	123 (8)	139 (2)	Geraniol
(+)-Neomenthol	11.21	71 (100)	81 (59)	109 (11)	123 (23)	138 (23)	(+)-Neomenthol
(−)-Menthol	11.48	71 (97)	81 (100)	109 (13)	123 (36)	138 (20)	(−)-Menthol
(−)-*trans*-Carveol	13.31	69 (23)	84 (60)	109 (100)	134 (4)	152 (7)	[47]
(−)-*cis*-Carveol	13.77	69 (40)	84 (100)	109 (63)	134 (42)	152 (2)	[47]
(−)-Neothujol	9.97	55 (94)	79 (58)	93 (100)	121 (53)	136 (18)	NMR
(−)-Thujol	10.51	55 (100)	79 (47)	93 (83)	121 (72)	136 (20)	NMR
(+)-α-Fenchol	9.99	81 (100)	93 (15)	111 (13)	121 (11)	139 (2)	(+)-α-Fenchol
(+)-β-Fenchol	10.15	81 (100)	93 (16)	111 (14)	121 (12)	139 (4)	(+)-α-Fenchol
(+)-Borneol	11.73	67 (10)	95 (100)	110 (20)	121 (6)	139 (6)	(−)-Borneol
Neral	13.56	69 (100)	94 (20)	109 (15)	119 (6)	137 (2)	Citral
(−)-Menthone	10.82	69 (91)	97 (33)	112 (100)	139 (36)	154 (22)	(−)-Menthone
(−)-Camphor	11.04	81 (77)	95 (100)	108 (45)	137 (4)	152 (26)	(+)-Camphor

Table 7
^{13}C (δ in ppm) and ^{1}H (δ in ppm, multiplicity, (J in Hz)) NMR data of (−)-α-thujone and corresponding alcohols (in $CDCl_3$).

Position	(−)-α-Thujone		(−)-Neothujol		(−)-Thujol	
	^{13}C	^{1}H	^{13}C	^{1}H	^{13}C	^{1}H
1	29.6	–	34.5	–	31.2	–
2	39.7	2.546 ddd (15.8;2.4;1.2) 2.071 d (18.8)	35.9	2.058 ddd (14.1;6.8;1.9) 1.532 dd (14.1;1.0)	33.4	1.933 dd (12.1;7.2) 1.556 ddd (12.1;9.1;1.3)
3	221.4	–	80.2	3.899 dddd (6.8;1.0;1.0;1.0)	72.6	3.943 ddd (9.1;7.2;7.0)
4	47.3	2.220 dq (7.5;1.2)	45.3	1.922 br q (7.3)	37.3	2.153 dq (7.1;7.0)
5	25.5	1.085 dd (8.1;4.0)	29.6	0.828 ddd (8.2;3.9;1.0)	28.2	0.858 dd (8.3;3.9)
6	18.7	0.762 ddd (8.1;5.6;2.4) 0.124 dd (5.6;4.0)	17.2	0.802 dd (4.2;3.9) 0.418 ddd (8.2;4.2;1.9)	14.4	0.351 dd (5.1;3.9) 0.231 ddd (8.3;5.1;1.3)
7	32.9	1.355 sept (6.9)	32.9	1.299 sept (6.9)	33.3	1.234 sept (6.9)
8[a]	19.7	1.008 d (6.9)	19.9	0.934 d (6.8)	19.6	0.961 d (6.9)
9[a]	20.0	0.954 d (6.9)	20.2	0.906 d (6.8)	20.1	0.905 d (6.9)
10	18.2	1.158 d (7.5)	20.1	0.940 d (7.3)	14.4	0.926 d (7.1)

[a] May be interchanged.

Table 8
Ramachandran plot analysis with PROCHECK and combined z-score resulting from PROSA II. Results of the Ramachandran plot are given as rates (%) of residues in most favored, additional allowed, generously allowed region. Glycines and prolines are not included in these rates.

Proteins	Most favoured	Additional allowed	Generously allowed	Combined z-score
At2g29350	90.6	8.1	1.3	−10.03
At2g29150	91.5	8.5	–	−9.71
At2g29330	92.5	7.5	–	−9.82
CoTR	92.5	7.5	–	−10.39

Detection was performed in a diode array detector. Compounds were identified comparing retention times and absorption spectra with standard compounds. Reduction products of flavanones and *trans*-chalcone were assigned using sodium borohydride reduced substrates.

4.6. NMR analysis of (−)-α-thujone reduction products

The product of (−)-α-thujone reduction catalyzed by CoTR was analyzed with ^{1}H NMR and ^{13}C NMR. A 10 mL assay with 5 mM NADPH, 3 mM (−)-α-thujone, 5% (v/v) methanol and 100 μg mL^{-1} CoTR in 100 mM citrate phosphate buffer pH 5.0 was incubated for 22.5 h at 30 °C. The assay was extracted four times with 2 mL n-hexane. Organic phases were combined and dried with Na_2SO_4. A 1:10 dilution of the assay extract was analyzed by GC–MS and contained about 25% (−)-α-thujone (Rt 8.65 min) and 75% of the alcohol product (Rt 10.51 min). After evaporation of n-hexane with nitrogen the residue was resolved in $CDCl_3$ for NMR measurements. An authentic standard of (−)-α-thujone and a mixture of equal amounts of sodium borohydride reduced (−)-α-thujone alcohols (1st alcohol Rt 9.97 min, 2nd alcohol Rt 10.51 min) were also analyzed. ^{1}H and ^{13}C NMR spectra were recorded on an Agilent V NMR 600 spectrometer (Varian) at 599.82 and 150.84 MHz, respectively. Chemical shifts were referenced to internal TMS (δ = 0 ppm, ^{1}H) and $CDCl_3$ (δ = 77.0 ppm, ^{13}C) (Table 7). Signal assignments were supported by 2D NMR measurements (DQFCOSY, HSQC, HMBC) and compared to available literature [36,37,48].

4.7. Homology modeling and virtual screening

Homology modeling of CoTR [17] used the template 1IPF [49] and MOE [50]. For modeling of the three *Arabidopsis* TRLs, the YASARA 11.4.18 2011 [51] Blastp search for template searching in the Protein Data Bank [1] provided five templates. Five crude homology models were generated and their quality was checked with PROCHECK [52] and PROSA II [53,54]. For all TRLs, the X-ray structure of tropinone reductase II from *Datura stramonium* (PDB ID 1IPE) [49] appeared as the best template with an amino acid sequence identity of about 50%. Molecular dynamic refinements (option of YASARA) were performed using the Yasara2 force field [55] with subsequent final energy minimizations with Amber03 [56]. Correct positioning of the active amino acids tyrosine and serine in the active site of the enzymes was achieved by manual docking of one reduced substrate in the active site and subsequent minimization using MOE with the PFROSST force field [57] and Born solvation [58]. The force field combines parameters for proteins and small molecules. All final models showed excellent stereo-chemical quality with no outlier in the Ramachandran plot and more than 90% of all amino acid residues in most favored areas (Table 8). The z-scores of combined energies resulting from the PROSA II analysis indicate a native like fold (Table 8).

For pharmacophore-guided identification of possible substrates the quality of the protein models especially in the active site was checked by docking of all monoterpenes, which had been experimentally proven to be substrates. For At2g29330, 1,4-cyclohexanedione was used, as this was the best substrate *in vitro* for the enzyme. Fifty docking runs were performed for each of these ligands using GOLD [59,60] with the GoldScore fitness function and for all other options with standard settings. For the definition of the active site the reactive hydrogen of NAD(P)H was chosen as origin. Since the distance of E216 in At2g29350 to the defined centre of the active site is larger than 10 Å standard setting, the

Table 9
Flexible side chains in the GOLD docking.

At2g29330	At2g29150	At2g29350	CoTR
R213	K221	–	–
L196	L204	L204	–
F200	I208	F208	Y209
F153	–	V161	V162
–	–	F108	–
–	–	E216[a]	–
–	–	–	F260

[a] Amino acid not flexible in docking in the screening route because of fixation with R219.

Table 10
Pharmacophore features in MOE for all enzymes, characteristics and radius.

Features	At2g29330	At2g29150	At2g29350
F1	Acceptor and not donor and not anion; 1.4 Å		
F2	Acceptor or hydrophobic; 1.6 Å	Hydrophobic; 1.7 Å	Hydrophobic; 1.8 Å
F3	Hydrophobic; 1.4 Å	Hydrophobic; 1.7 Å	Hydrophobic; 1.8 Å
F4	Hydrophobic; 1.8 Å	Hydrophobic; 1.8 Å	Hydrophobic; 1.8 Å
F5	Acceptor or hydrophobic; 1.4 Å	Acceptor; 1.0 Å	Hydrophobic; 1.8 Å

binding regions were enhanced to 12 Å. Some amino acid side chains (Table 9) were set to be flexible applying the rotamer library included in GOLD.

The docking results were analyzed manually looking for conformations which were in a reactive position, e.g. the carbonyl group to be reduced formed hydrogen bonds with the active sites tyrosine and serine. Based on these docking arrangements for the best-converted monoterpene substrates and the stereo-chemical and electronic properties of the active site of each enzyme, pharmacophores (Fig. 8, and Table 10) with excluded volumes were created using MOE. The 3D Leadlike Conformer Database of MOE provided 650,000 commercially available structures. Those with carbonyl functions and a molecular weight <400 Da were selected (365,284 structures) and screened by the pharmacophores for binding. All hits from the pharmacophore search (Fig. 8, step 1) were docked with GOLD (Fig. 8, step 2), and 10 conformations were created and early termination was allowed. After docking, a second search with the same pharmacophore without excluded volumes identified those ligand conformations, which obeyed to feature 1 (binding carboxyl oxygen) as essential feature (Fig. 8, third column, step 2) and matched at least four out of five features. Figures of homology models and pharmacophores were designed with MOE.

Acknowledgments

Anja Plohmann, Institute of Pharmacy, MLU, helped with cloning and protein synthesis of At2g29150. We thank Dr. Andrea Porzel, Leibniz Institute of Plant Biochemistry Halle, for excellent NMR measurements and helpful discussions. Experiments were financially supported by the German Research Foundation (BR 1329, DR 227).

Appendix A. Supplementary material

Supplementary data associated with this article can be found, in the online version, at http://dx.doi.org/10.1016/j.bioorg.2014.01.004.

References

[1] Y. Kallberg, U. Oppermann, B. Persson, FEBS J. 277 (2010) 2375–2386.
[2] H.M. Berman, J. Westbrook, Z. Feng, G. Gilliland, T.N. Bhat, H. Weissig, I.N. Shindyalov, P.E. Bourne, Nucleic Acids Res. 28 (2000) 235–242.
[3] B. Persson, Y. Kallberg, J.E. Bray, E. Bruford, S.L. Dellaporta, A.D. Favia, R.G. Duarte, H. Jörnvall, K.L. Kavanagh, N. Kedishvili, M. Kisiela, E. Maserk, R. Mindnich, S. Orchard, T.M. Penning, J.M. Thornton, J. Adamski, U. Oppermann, Chem. Biol. Interact. 178 (2009) 94–98.
[4] K. Kavanagh, H. Jörnvall, B. Persson, U. Oppermann, Cell. Mol. Life Sci. 65 (2008) 3895–3906.
[5] U. Oppermann, C. Filling, M. Hult, N. Shafqat, X.Q. Wu, M. Lindh, J. Shafqat, E. Nordling, Y. Kallberg, B. Persson, H. Jörnvall, Chem. Biol. Interact. 143 (2003) (2002) 247–253.
[6] Y. Kallberg, U. Oppermann, H. Jörnvall, B. Persson, Eur. J. Biochem. 269 (2002) 4409–4417.
[7] C. Filling, K.D. Berndt, J. Benach, S. Knapp, T. Prozorovski, E. Nordling, R. Ladenstein, H. Jörnvall, U. Oppermann, J. Biol. Chem. 277 (2002) 25677–25684.
[8] R. Geissler, W. Brandt, J. Ziegler, Plant Physiol. 143 (2007) 1493–1503.
[9] A.D. Favia, I. Nobeli, F. Glaser, J.M. Thornton, J. Mol. Biol. 375 (2008) 855–874.
[10] B. Dräger, Phytochemistry 67 (2006) 327–337.
[11] A. Brock, T. Herzfeld, R. Paschke, M. Koch, B. Dräger, Phytochemistry 67 (2006) 2050–2057.
[12] H.W. Liebisch, H. Bernasch, H.R. Schütte, Z. Chem. 13 (1973) 372–373.
[13] The UniProt Consortium, Reorganizing the protein space at the Universal Protein Resource (UniProt), Nucleic Acids Res. 40 (2012) D71–D75.
[14] W. Chen, X. Cheng, Z. Zhou, J. Liu, H. Wang, Mol. Biol. Rep. 40 (2013) 1145–1154.
[15] K. Nakajima, A. Yamashita, H. Akama, T. Nakatsu, H. Kato, T. Hashimoto, J. Oda, Y. Yamada, Proc. Natl. Acad. Sci. USA 95 (1998) 4876–4881.
[16] K. Nakajima, H. Kato, J. Oda, Y. Yamada, T. Hashimoto, J. Biol. Chem. 274 (1999) 16563–16568.
[17] A. Brock, W. Brandt, B. Dräger, Plant J 54 (2008) 388–401.
[18] M.A. Larkin, G. Blackshields, N.P. Brown, R. Chenna, P.A. McGettigan, H. McWilliam, F. Valentin, I.M. Wallace, A. Wilm, R. Lopez, J.D. Thompson, T.J. Gibson, D.G. Higgins, Bioinformatics 23 (2007) 2947–2948.
[19] B. Dräger, A. Schaal, Phytochemistry 35 (1994) 1441–1447.
[20] T. Hashimoto, K. Nakajima, G. Ongena, Y. Yamada, Plant Physiol. 100 (1992) 836–845.
[21] Y. Kallberg, B. Persson, FEBS J. 273 (2006) 1177–1184.
[22] A. Portsteffen, B. Dräger, A. Nahrstedt, Phytochemistry 31 (1992) 1135–1138.
[23] J. Benach, C. Filling, U.C.T. Oppermann, P. Roversi, G. Bricogne, K.D. Berndt, H. Jornvall, R. Ladenstein, Biochemistry 41 (2002) 14659–14668.
[24] Y.H. Chang, L.Y. Chuang, C.C. Hwang, J. Biol. Chem. 282 (2007) 34306–34314.
[25] J.K. Lee, B.S. Koo, S.Y. Kim, H.H. Hyun, Appl. Environ. Microbiol. 69 (2003) 4438–4447.
[26] B. Sahni-Arya, M.J. Flynn, L. Bergeron, M.E.K. Salyan, D.L. Pedicord, R. Golla, Z.P. Ma, H.X. Wang, R. Seethala, S.C. Wu, J.J. Li, A. Nayeem, C. Gates, L.G. Hamann, D.A. Gordon, Y. Blat, BBA-Proteins Proteomics 1774 (2007) 1184–1191.
[27] C.E. Grimshaw, K.M. Bohren, C.J. Lai, K.H. Gabbay, Biochemistry 34 (1995) 14356–14365.
[28] T.J. Kubiseski, D.J. Hyndman, N.A. Morjana, T.G. Flynn, J. Biol. Chem. 267 (1992) 6510–6517.
[29] G. Bhabha, J. Lee, D.C. Ekiert, J. Gam, I.A. Wilson, H.J. Dyson, S.J. Benkovic, P.E. Wright, Science 332 (2011) 234–238.
[30] M. Nakanishi, K. Matsuura, H. Kaibe, N. Tanaka, T. Nonaka, Y. Mitsui, A. Hara, J. Biol. Chem. 272 (1997) 2218–2222.
[31] N. Trabelsi, B. Langlois d'Estaintot, G. Sigaud, B. Gallois, J. Chaudiere, JBPC 2 (2011) 332–344.
[32] J. Rohloff, A.M. Bones, Phytochemistry 66 (2005) 1941–1955.
[33] L. Tollsten, G. Bergström, Phytochemistry 27 (1988) 4013–4018.
[34] E.M. Davis, K.L. Ringer, M.E. McConkey, R. Croteau, Plant Physiol. 137 (2005) 873–881.
[35] A.-M. Ryden, C. Ruyter-Spira, R. Litjens, S. Takahashi, W. Quax, H. Osada, H. Bouwmeester, O. Kayser, Plant Cell Physiol. 51 (2010) 1219–1228.
[36] P. Baeckström, B. Koutek, D. Saman, J. Vrkoc, Bioorg. Med. Chem. 4 (1996) 419–421.
[37] F. Bohlmann, R. Zeisberg, E. Klein, Org. Magn. Reson. 7 (1975) 426–432.
[38] Y. Arellano, E. Bratoeff, M. Garrido, J. Soriano, Y. Heuze, M. Cabeza, Steroids 76 (2011) 1241–1246.
[39] K. Kristan, S. Starcevic, M. Brunskole, T.L. Rizner, S. Gobec, Mol. Cell. Endocrinol. 248 (2006) 239–241.
[40] K. Kristan, J. Stojan, G. Moller, J. Adamski, T.L. Rizner, Mol. Cell. Endocrinol. 241 (2005) 80–87.
[41] B. Petschacher, B. Nidetzky, Microb. Cell Fact. 7 (2008).
[42] N.H. Schlieben, K. Niefind, J. Müller, B. Riebel, W. Hummel, D. Schomburg, J. Mol. Biol. 349 (2005) 801–813.
[43] A. Nickon, L.F. Fieser, J. Am. Chem. Soc. 74 (1952) 5566–5570.
[44] C. Reinbothe, A. Tewes, M. Luckner, S. Reinbothe, Plant J. 2 (1992) 917–926.
[45] U.K. Laemmli, Nature 227 (1970). 680-&.
[46] M.M. Bradford, Anal. Biochem. 72 (1976) 248–254.
[47] M.J. van der Werf, C. van der Ven, F. Barbirato, M.H.M. Eppink, J.A.M. de Bont, W.J.H. van Berkel, J. Biol. Chem. 274 (1999) 26296–26304.
[48] N.S. Sirisoma, K.M. Hold, J.E. Casida, J. Agric. Food Chem. 49 (2001) 1915–1921.
[49] A. Yamashita, M. Endo, T. Higashi, T. Nakatsu, Y. Yamada, J. Oda, H. Kato, Biochemistry 42 (2003) 5566–5573.
[50] Chemical Computing Group Inc., in: Molecular Operating Environment (MOE), 2011.10, 2011).

[51] E. Krieger, G. Koraimann, G. Vriend, Proteins 47 (2002) 393–402.
[52] R.A. Laskowski, M.W. Macarthur, D.S. Moss, J.M. Thornton, J. Appl. Crystallogr. 26 (1993) 283–291.
[53] M.J. Sippl, J. Mol. Biol. 213 (1990) 859–883.
[54] M.J. Sippl, Proteins 17 (1993) 355–362.
[55] E. Krieger, K. Joo, J. Lee, J. Lee, S. Raman, J. Thompson, M. Tyka, D. Baker, K. Karplus, Proteins 77 (Suppl 9) (2009) 114–122.
[56] Y. Duan, C. Wu, S. Chowdhury, M.C. Lee, G. Xiong, W. Zhang, R. Yang, P. Cieplak, R. Luo, T. Lee, J. Caldwell, J. Wang, P. Kollman, J. Comput. Chem. 24 (2003) 1999–2012.
[57] C.I. Bayly, D. McKay, J.-F. Truchon, Parm@frosst Small Molecule Parameters Compatible with AMBER, Merck & Co. Internal Development Release, 2011.
[58] M. Wojciechowski, B. Lesyng, J. Phys. Chem. B 108 (2004) 18368–18376.
[59] M.J. Hartshorn, M.L. Verdonk, G. Chessari, S.C. Brewerton, W.T. Mooij, P.N. Mortenson, C.W. Murray, J. Med. Chem. 50 (2007) 726–741.
[60] M.L. Verdonk, J.C. Cole, M.J. Hartshorn, C.W. Murray, R.D. Taylor, Proteins 52 (2003) 609–623.